National University of Science and Technology POLITEHNICA Bucharest

Doctoral School of ENERGY ENGINEERING

Senate decision no. 141/22.11.2023

PHD THESIS SUMMARY

NEUTRONIC ANALYSIS OF A FAST LIQUID METAL COOLED REACTOR

Author: Eng. Andreea MOISE

DOCTORAL COMMITTEE

Chairman	Prof. dr. eng. Radu PORUMB	from	National University of Science and Technology POLITEHNICA Bucharest
PhD Supervisor	Prof. dr. eng. Daniel DUPLEAC	from	National University of Science and Technology POLITEHNICA Bucharest
Reviewer	CS II dr. eng. Marin CONSTANTIN	from	Institute for Nuclear Research Pitești
Reviewer	CS II dr. eng. Radu VASILE	from	Institute for Nuclear Research Pitești
Reviewer	Conf. dr. eng. Cătălin Marian DUCU	from	National University of Science and Technology POLITEHNICA Bucharest (Pitești)

Bucharest, 2023

MOTIVATION

The decision to explore new nuclear reactor concepts in my doctoral thesis, focusing on liquid metal-cooled fast reactors, stems from a solid set of personal motives and scientifically significant considerations.

Commitment to the Environment: As climate change poses a global challenge, reducing carbon emissions is crucial for protecting the environment. Aware of this challenge, I believe that nuclear energy, especially in the context of new reactor concepts, can be crucial in providing a low-carbon energy source.

Contribution to the Future: I feel responsible for leaving future generations with a cleaner and more sustainable planet. By concentrating on researching and developing new nuclear reactor concepts, I aim to contribute to developing technologies that ensure a sustainable long-term energy source for our society.

Interest in Innovation: As interested in innovative technologies, I consider liquid metal-cooled nuclear reactors to be a promising direction in nuclear energy. This thesis has provided me with an opportunity to deepen my knowledge and contribute to the advancement of these revolutionary technologies.

Global Relevance: Collaborating with the Institute of Atomic Energy from China and participating in the Coordinated Research Project (CRP) under the guidance of the International Atomic Energy Agency (IAEA) underscores the recognition of my research at the international level. This collaboration not only enriches the exchange of knowledge but also brings significant benefits to the joint approach to global issues related to nuclear energy.

Personal and Professional Development: Exploring this complex subject will develop my advanced research, analysis, and simulation skills, allowing me to work in an international environment and learn from experts in the field. This experience will significantly contribute to my evolution as a researcher in the energy sector.

In conclusion, the fundamental reason for my choice was to make a concrete contribution to developing sustainable energy solutions, using my knowledge and dedication to address energy and environmental challenges. This thesis represents an essential step in the direction of this journey.

CONTENT

Keywords: fast reactor, liquid metals, neutronics, Monte Carlo codes, reactivity effects, nuclear data libraries.

1. INTRODUCTION

Chapter 1 addresses several key aspects related to climate change and global energy challenges. The topic is grounded in the current context, highlighting the significant impact of climate change and the need for an energy transition. The thesis first explores the importance of reducing carbon emissions to avoid excessive global warming, as IPCC reports indicate [1].

The research also emphasizes the geopolitical context, showing that traditional fossil fuel resources cannot meet long-term energy demand. It further highlights that nuclear energy and renewable sources play an essential role in providing globally low-carbon energy.

The thesis argues that despite progress in renewable energies, they are insufficient to meet the growing global energy demand due to limitations such as intermittency and the inability to store energy for the long term [2].. Nuclear energy is presented as a necessary and efficient alternative, capable of providing constant energy regardless of weather conditions.

An important aspect discussed is recent changes in Europe's energy policy, where nuclear energy is reconsidered as a zero-carbon energy source. The thesis emphasizes that some European countries, including Romania, have announced plans to build new nuclear reactors to meet decarbonization goals.

In the section dedicated to nuclear energy production and its role in the current context, the thesis presents the number of existing units and those under construction. It is noted that despite incidents like Fukushima, interest in nuclear energy is returning due to the need to achieve climate goals and technological advancements quickly [3].

Chapter 1 also highlights the main characteristics a Generation IV reactor must fulfill, focusing on improving energy production efficiency and increasing nuclear safety. These characteristics include sustainability, economic competitiveness, safety and reliability, non-proliferation, and efficient use of nuclear fuel resources.

The thesis identifies six Generation IV reactor concepts supported by the Generation IV International Forum (GIF) [4]:

- SCWR (Supercritical Water-cooled Reactor);

- VHTR (Very High Temperature Reactor);

- GFR (Gas-cooled Fast Reactor);

- MSR (Molten Salt Reactor);

- LFR (Lead-cooled Fast Reactor);

- SFR (Sodium-cooled Fast Reactor).

The section focuses on the characteristics and potential of the Sodium-cooled Fast Reactor (SFR), highlighting the fast neutron spectrum, the temperature of the cooling agent (liquid sodium), the closed fuel cycle, and possible reactor configurations. It underscores the

technological maturity of the SFR technology, citing operational experience in various countries and planned projects for the future [5].

Safety aspects of the SFR technology are also discussed, including risks associated with sodium chemical reactions with air and water, coolant solidification, and embrittlement of steels in the presence of sodium [6]. However, it emphasizes that SFR technology offers significant benefits such as efficient use of nuclear fuel, minimization of radioactive waste, inherent safety features, and economic competitiveness.

Despite technological maturity, the thesis acknowledges aspects that require further study, including passive systems, capital cost reduction, reactor safety, minor actinide burning, and the development of MOX fuel technology [7]. Nevertheless, SFR is presented as an attractive option for countries interested in efficiently utilizing limited nuclear fuel resources and managing radioactive waste through a closed fuel cycle.

2. NEUTRON TRANSPORT THEORY AND CALCULATION METHODS

Chapter 2 focuses on the challenges related to the design of nuclear reactors, emphasizing predicting neutron and photon distributions throughout all reactor components. These distributions must consider space, angle, energy, and time, considering the impact of neutrons and photons on chain reactions, thermo-mechanical responses, and structural component degradation [8].

The transport equation [9], a form of the Boltzmann equation describing radiation transport through matter, is employed to address this challenge. Two main approaches for solving the neutron transport equation are the integro-differential approach and the completely integral approach [10].

The chapter details the neutron transport equation, describing their movement under the influence of atomic nuclei, involving scattering, capture, and fission events. The integro-differential and integral equations are presented, focusing on neutron interactions with nuclei. Within the context of the neutron transport equation, which is crucial for understanding neutron behavior in different environments, the advantages and disadvantages of each approach are explored.

The methods and calculation codes used to solve the transport equation are presented, highlighting both deterministic methods [11] and Monte Carlo (MC) methods [12].

Deterministic methods involve discretizing spatial and angular variables, relying on structured nodes that may require complex problem approximations. To overcome these limitations, deterministic methods with unstructured nodes are developed. In contrast, MC methods track neutrons in real geometric structures, offering high adaptability but may involve extended computation times.

The thesis discusses combining both codes in a calculation routine to maximize simulation efficiency. The choice between deterministic and MC methods depends on the nature of the analyzed problem, each having specific advantages and disadvantages. Deterministic methods focus on aspects such as neutronics, thermal-hydraulics, thermomechanics, structural, and radiological, aiming to confirm reactor safety and efficiency. Meanwhile, MC methods provide statistically accurate simulations of the model, with advantages such as continuous energy treatment and exact 3D geometry modeling.

The validation and verification of calculation codes are emphasized as essential, and previous studies, as mentioned [13], [14], [15], have been conducted to demonstrate the validity of these codes. It is highlighted that the demand for precise numerical solutions to the neutron transport equation is increasing with the rapid development of advanced nuclear reactor concepts and high-performance computing technologies.

In conclusion, two Monte Carlo-type codes, SERPENT 2 [16] and MCNP 6.2 [17], are present within the doctoral thesis, along with their specific advantages and characteristics used for nuclear reactor simulations.

3. REACTIVITY EFFECTS

Chapter 3 focuses on the impact of temperature on the reactivity of a nuclear reactor. It is mentioned that a large number of neutrons in a reactor generate temperature variations in various materials inside it, affecting reactivity. An increase in the number of neutrons leads to an increase in the heat generated through fission, affecting the temperature of the fuel element. Subsequent changes in the temperature of the coolant, moderator, and other structural elements are also discussed. Effects such as the Doppler Effect, changes in absorption cross-sections, and modifications in reactor geometry are presented as factors influencing reactivity.

To quantify reactivity changes with temperature, the thesis mentions the use of reactivity temperature coefficients, denoted as α_T [18]. These coefficients are defined and explored in detail. The importance of obtaining temperature coefficients with negative values is emphasized for the safety of nuclear reactors.

Chapter 3 also describes the state of a reactor in terms of the reactivity of the active core, power, and temperature. It is mentioned that temperature influences the reactor power, and two main mechanisms that can cause reactivity variations are discussed: deliberate actions by the operator and thermal effects.

It is emphasized that a system is stable when the temperature coefficient is negative and unstable when it is positive. Distinctions are made between materials used in the reactor in terms of reactivity coefficients, as these can vary significantly.

The Doppler Effect in the fuel is discussed in detail, highlighting its importance in ensuring reactor stability. The phenomenon is linked to changes in microscopic cross-sections caused by the thermal motion of atoms. The Doppler coefficient has a negative value and contributes to reactor stability because an increase in temperature leads to an increase in neutron absorption, resulting in a decrease in reactivity.

The thesis also addresses other thermal effects, such as changes in coolant density and the fuel's radial and axial thermal expansion and cladding. Their impact on reactivity is discussed in detail, highlighting positive or negative feedback associated with them.

In conclusion, it is emphasized that thermal effects may have certain peculiarities for fast reactors, such as minimizing neutron moderation. It is concluded that a clear understanding of these thermal effects and accurate modeling of their influence on the reactor is essential for the efficient and safe design of nuclear reactors.

4. CEFR DESCRIPTION

Chapter 4 presents the description of the China Experimental Fast Reactor (CEFR). CEFR [19] is a fast sodium-cooled reactor with a nominal thermal power of 65 MWt (20 MWe). It was connected to the electrical power grid in July 2011, featuring a pool-type configuration and utilizing three loops (sodium-sodium-water). It operates with oxide-based fuel, including uranium oxide and mixed plutonium-uranium oxide. The key parameters of the CEFR reactor are presented in Table 4.1 [20].

Table 4.1. Main Parameters of the CEFR Reactor.

Parameter	**Value**
Diameter/Height of the reactor vessel (m)	8/12.2
Coolant Inlet/Outlet Temperature from the active core (°C)	360/530
Maximum Flux ($cm^{-2}s^{-1}$)	3.2×10^{15}
Nominal Thermal/Electric Power (MW)	65/20
Maximum Burnup (MWd/t)	60000
Refueling Period (days)	80
Lifetime (years)	30

The CEFR active core configuration was designed to allow operation with two different types of fuel: uranium oxide fuel with enrichment of 64.4% in ^{235}U and MOX fuel. The active core configuration used for conducting the reactor start-up tests is presented in Figure 4.1.

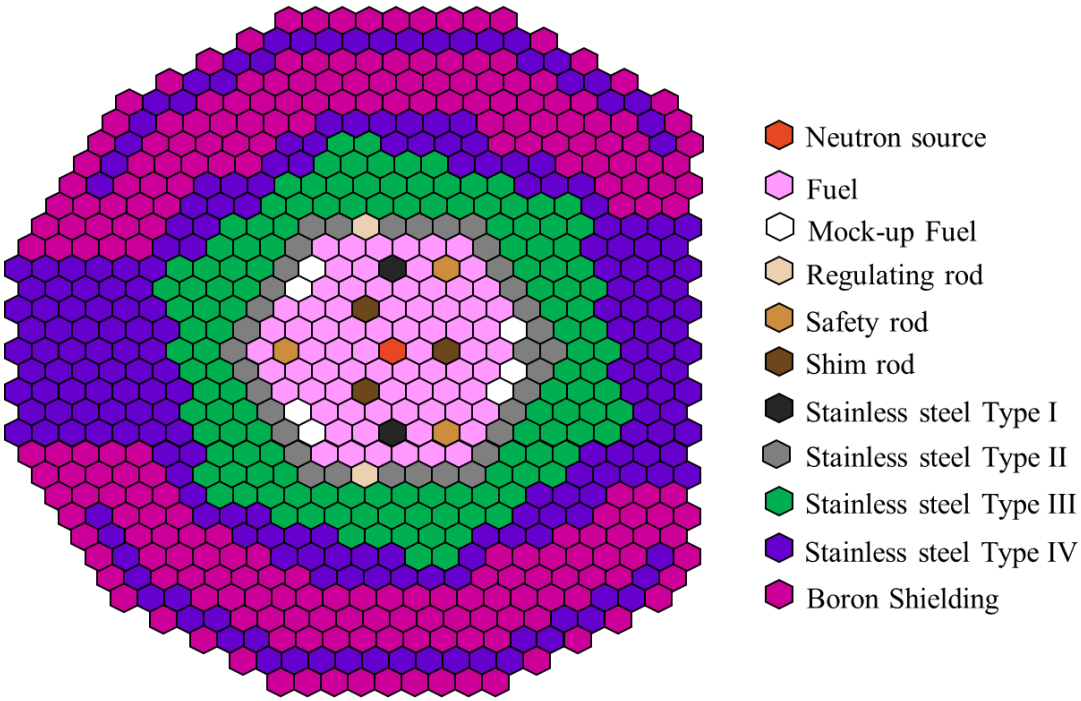

Figure 4.1: The active core configuration of the CEFR.

The geometric details of the assemblies, including length, diameter, composition, and mass, are presented in Table 4.2. The values are established for all component materials at a temperature of 20°C [20].

Table 4.2. Key Parameters of the Assemblies.

	NS	FA		CR		SS		BS
		Fissile	Fertile	RE	SH/SA	Type I-II	Type III-IV	
Number	1	79		2	3+3	39	355	230
Length (mm)	2580	2592		2580		2592	2592	2592
Active length (mm)	N/A	450	100/250	510		N/A	N/A	800
Inner Pencil Diameter (mm)	N/A	5.4		12.9		N/A	N/A	17.2
Outer Pencil Diameter (mm)	20.0	6.0		14.9		20.0	54.0	19.2
Spacer Diameter (mm)	1.3×0.6	0.95		1.3×0.6		0.6	N/A	0.95
Spacer Length (mm)	100	100		100		100	N/A	100
Number of Pencils	7	61		7		7	1	7
Grid Pitch (mm)	20.7	6.95		15.5		20.6	N/A	20.15
Material/Enrichment		UO_2		B_4C				
	^{252}Cf	64.4±0.5 wt% ^{235}U	0.3-0.7 wt% ^{235}U	19.6 a%^{10}B	92.0 a%^{10}B	^{316}Ti	^{316}Ti	19.8a% ^{10}B
Effective Material Mass (kg)	0.43E-6	5.3±0.13	1.28/3.23	0.87		N/A	N/A	2.43
Total mass (kg)	39~41	29~31		22~23		41~43	42~44	31~33

The importance of adjusting parameters for different temperatures using specified linear expansion coefficients is mentioned. Table 4.3 provides linear expansion coefficients for recalculating geometric parameters at different temperatures.

Table 4.3. Linear Expansion Coefficients.

Material	Coefficient ($°C^{-1}$)
Fissile	1.1×10^{-5}
Fertile	1.0×10^{-5}
Absorbent	4.2×10^{-6}
Steel	1.8×10^{-5}

This chapter provides essential details regarding the component assemblies of the CEFR reactor, including fuel assemblies, control assemblies, steel assemblies, boron assemblies, neutron source, and the coolant.

5. RESULTS AND DISCUSSION

5.1. Description of the simulated models

Chapter 5 focuses on neutron simulations of the start-up tests of CEFR. The purpose of the simulations is to predict the behavior of neutrons under static conditions, with the main objective of critical parameters such as the effective multiplication factor (k_{eff}), radial power distribution, reactivity induced by control systems, and others.

In the thesis, two Monte Carlo codes, SERPENT 2 and MCNP 6.2, were successfully used for neutron analyses essential for the CEFR. The complex modeling of the reactor's geometry involved detailing operating conditions, defining geometry, and materials. Simulations were performed under zero power conditions, with a uniform temperature of 250°C in the active core.

The geometry modeling was based on the "universe" concept in Monte Carlo codes, using the Constructive Solid Geometry method. The active core was divided into 16 types of assemblies, each defined as a separate "universe". The modeling was done hierarchically, from outer to inner, following the natural levels of geometry. Figure 5.1 illustrates the four hierarchical levels of the CEFR reactor's active core model.

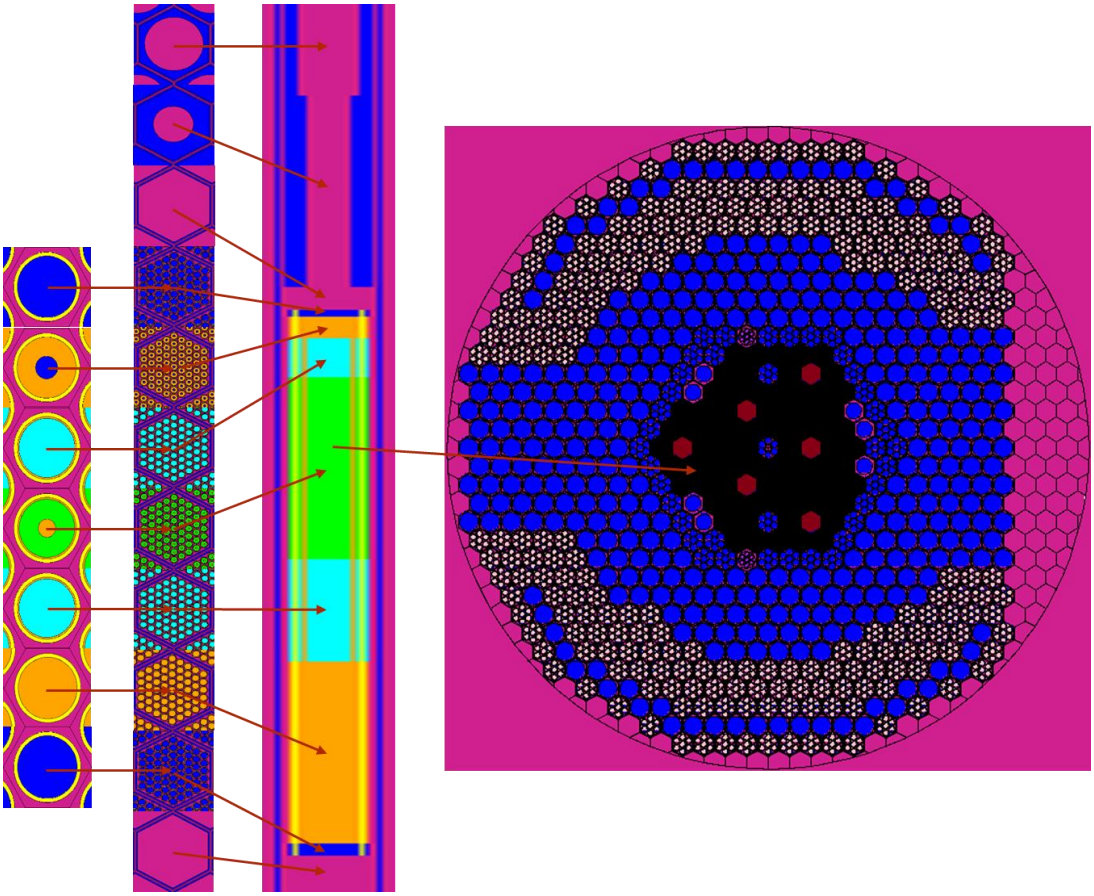

Figure 5.1: The Hierarchical Levels Followed in Constructing the CEFR Geometry.

The preparation of input data involved collecting and processing information regarding operating conditions, geometry, and materials. Material densities were adjusted to the operating temperature using linear thermal expansion coefficients.

5.2. Fuel loading and the first criticality

The chapter describes the fuel loading process in the CEFR reactor before its physical start-up. In the initial phase, the active core was loaded with pseudo-fuel assemblies (MF), having a total mass nearly identical to the fuel assemblies (FA). The purpose of this stage was to test feeding and transport mechanisms, as well as to filter impurities from sodium that might have been introduced during installation.

The reactor achieved first criticality by successively replacing pseudo-fuel assemblies with fuel assemblies following a detailed scheme presented in Table 5.1 [20]. The active core became supercritical after loading 72 fuel assemblies. A control assembly (RE2) was introduced to attain the critical state and then gradually withdrawn into three different positions, reaching the final critical state known as the "clean core." This state is characterized by achieving criticality with minimal fuel assemblies and with most control systems located outside the active core.

Table 5.1. Loading Scheme for Achieving First Criticality in the Reactor.

Step	Control rod position, RE2 [mm]	Fuel assemblies loaded	Reactor state
1-9	500	24, 40*, 46, 55, 61, 65, 68, 69, 70	Subcritical
10	500	71	End of subcritical state
11	190	72	Supercritical
12	170	72	Supercritical
13	151	72	Supercritical
14	70	72	Critical

**After loading 40 fuel assemblies, two pseudo-fuel assemblies are replaced with two Type I steel assemblies.*

In the thesis, the simulation results for the last six fuel loading steps were presented, and they are found in Table 5.2. We conducted these simulations to monitor this crucial reactor operation process.

Table 5.2. Multiplication Factor Obtained for the First Fuel Loading.

Step	Fuel assemblies loaded	Control rod position, RE2 [mm]	k_{eff} (Std. Dev.)		
			Experimental	SERPENT 2 (±4.3pcm)	MCNP 6.2 (±6pcm)
9	70	500	-	0.99363	0.99355
10	71	500	-	0.99790	0.99786
11	72	190	1.00040	1.00142	1.00130
12	72	170	1.00034	1.00122	1.00119
13	72	151	1.00025	1.00117	1.00113
14	72	70	1.00000	1.00098	1.00088

The use of a heterogeneous model led to a notable convergence between the numerical results obtained from simulations with SERPENT 2 and MCNP 6.2 and the measured experimental data [21]. The comparison between experimental results, in terms of reactivity excess, for the last four loading steps and the numerical results obtained with SERPENT 2 and MCNP 6.2 is presented in Figure 5.2.

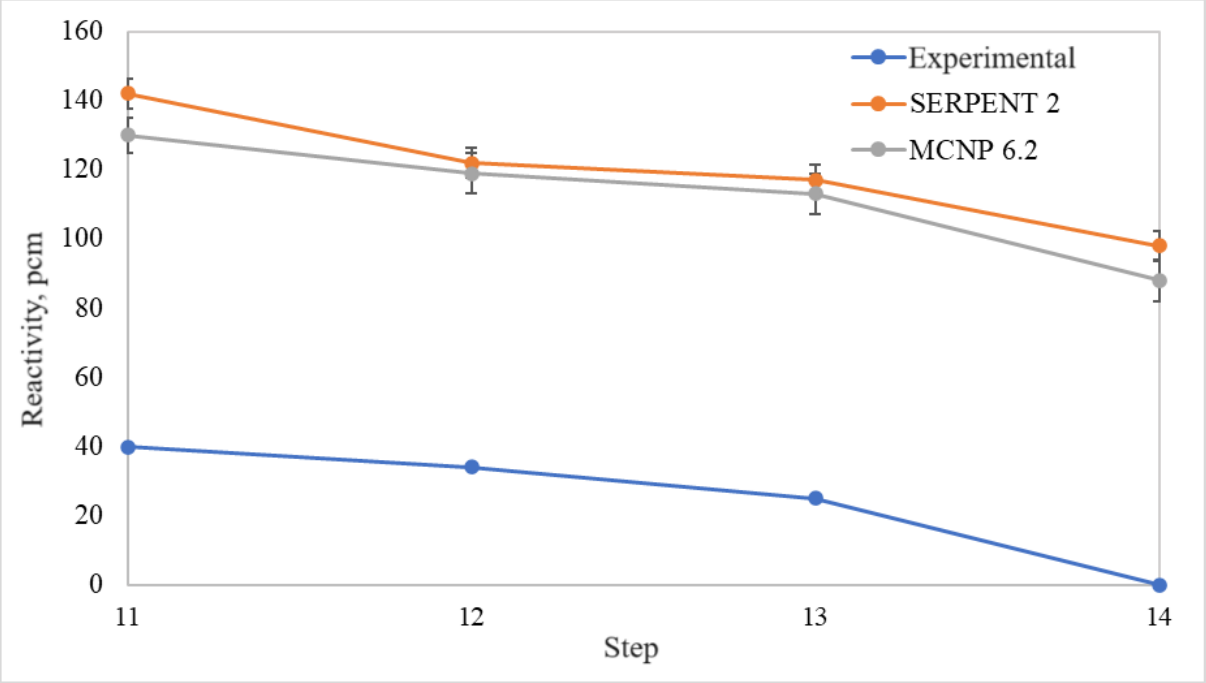

Figure 5.2: Evolution of Reactivity Excess before Achieving First Criticality.

I emphasize that the transition process from subcritical to supercritical state was achieved in well-defined stages, highlighting the agreement between simulated and experimental results. The observed differences are consistent and reflect similar behavior, thus validating the accuracy of the simulations in the context of the CEFR reactor's operation.

5.3. Control reactivity worth

This chapter focuses on determining the effectiveness of control systems during the start-up process of the CEFR reactor, providing crucial information for ensuring its safe operation. Experimental measurements involved replacing 81 pseudo-fuel assemblies with 79 fuel assemblies and 2 Type I steel assemblies. The effectiveness of control assemblies was evaluated through tests that included normal operation and their release by free fall.

In the first stage, we determined the control rod worth when the other rods are fully withdrawn from the active core. Two Monte Carlo codes, SERPENT 2 and MCNP 6.2, were used to calculate the reactivity of the control assemblies. The obtained results are presented in Figure 5.3.

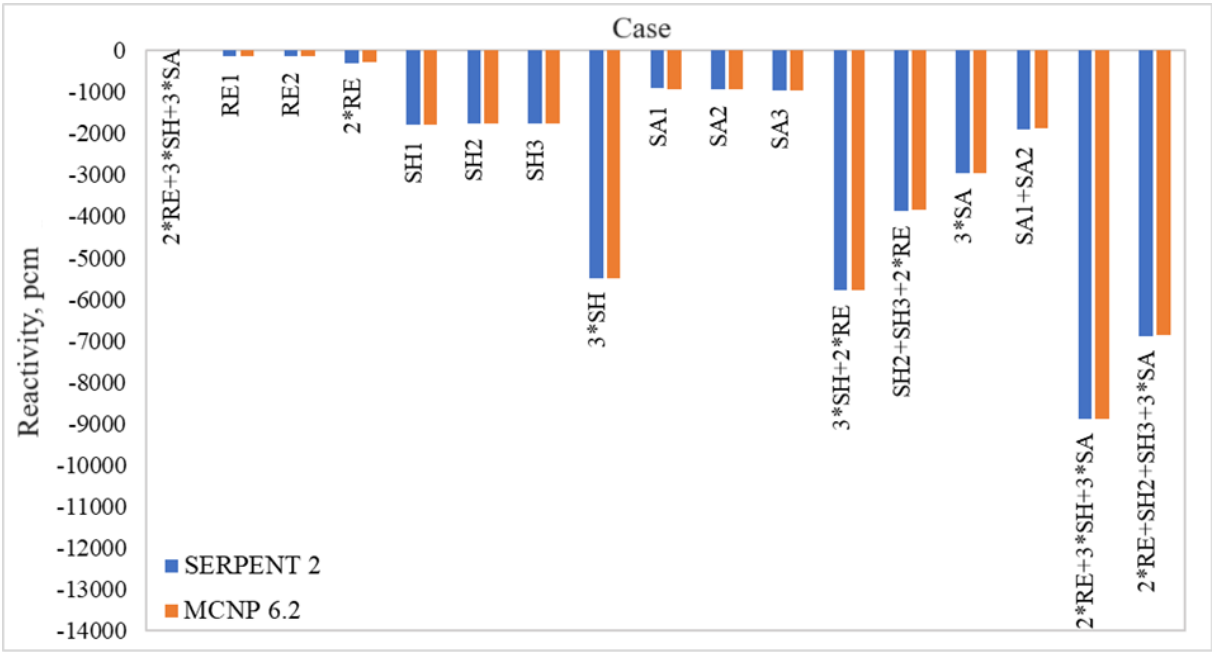

Figure 5.3: Control rods worth upon complete insertion into the active core.

The results in Figure 5.3 indicate notable consistency between the two codes. It is observed that the regulating rod contributes to a negative reactivity of approximately -145pcm, shim rod induces a significant negative reactivity of -1770pcm, and the safety rod results in an average negative reactivity of -940pcm. These data provide insight into how control assemblies influence the reactor's multiplication factor in various configurations.

In the second stage, we determined the control rod worth considering the exact positions of the other assemblies. A detailed comparison between simulations and experimental results was conducted. Table 5.3 provides the reactivity induced by each assembly in different reactor configurations. The results indicate consistency between the two evaluation stages and validate the reactor models used. This detailed assessment contributes to a deeper understanding of the reactor's behavior based on the position of each control assembly, which is crucial for optimizing operation and ensuring safety under various conditions.

Table 5.3. Reactivity induced by a control assembly/group of assemblies.

Case	Inserted rod	State	k_{eff}		$\Delta\rho$ (Std. dev.) [pcm]		
			SERPENT 2	MCNP 6.2	SERPENT 2 (±6pcm)	MCNP 6.2 (±8.5pcm)	Experimental
1	RE1	Before	1.00333	1.00327	-155	-152	-150(±9)
		After	1.00177	1.00174			
2	RE2	Before	1.00320	1.00316	-146	-145	-149(±9)
		After	1.00173	1.00170			
3	SH1	Before	1.00222	1.00209	-1901	-1896	-2019(±250)
		After	0.98348	0.98341			
4	SH2	Before	1.00266	1.00262	-1844	-1839	-1839(±225)
		After	0.98446	0.98447			
5	SH3	Before	1.00248	1.00235	-1833	-1833	-1839(±226)
		After	0.98439	0.98427			
6	SA1	Before	1.00312	1.00303	-889	-881	-945(±100)
		After	0.99425	0.99424			
7	SA2	Before	1.00313	1.00292	-868	-852	-911(±100)
		After	0.99447	0.99442			

Case	Inserted rod	State	k_{eff}		$\Delta\rho$ (Std. dev.) [pcm]		
			SERPENT 2	MCNP 6.2	SERPENT 2 (±6pcm)	MCNP 6.2 (±8.5pcm)	Experimental
8	SA3	Before	1.00310	1.00303	-940	-932	-946(±98)
		After	0.99373	0.99374			
9	3×SH+2×RE	Before	1.00319	1.00303	-3029	-3029	-2877(±335)
		After	0.97361	0.97345			
10	SH2+SH3+2×RE	Before	1.00221	1.00214	-997	-991	-881(±76)
		After	0.99230	0.99229			
11	3×SA	Before	1.00320	1.00322	-2845	-2855	-2981(±395)
		After	0.97536	0.97529			
12	SA1+SA2	Before	1.00323	1.00322	-1806	-1819	-1950(±226)
		After	0.98538	0.98524			
13	2×RE+3×SH+3×SA	Before	1.00320	1.00317	-5995	-6004	-6079(±989)
		After	0.94629	0.94618			
14	2×RE+SH2+SH3+3×SA	Before	1.00225	1.00209	-3896	-3898	-3899(±551)
		After	0.96459	0.96442			

The integral and differential reactivity results, presented in Figure 5.4, are analyzed using nonlinear mathematical functions to highlight how reactivity varies depending on the position of the control assemblies. This analysis significantly contributes to a detailed understanding of how control assemblies influence reactivity and reactor power control.

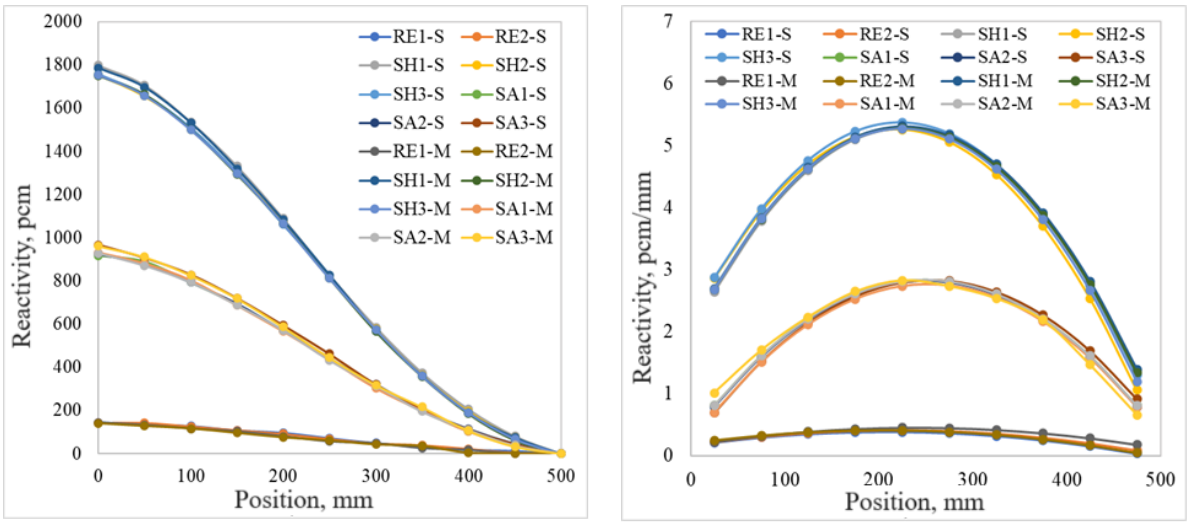

Figure 5.4: Integral Reactivity (left) and Differential Reactivity (right).

This comprehensive and detailed approach emphasizes the consistency and relevance of the calculation methods used, contributing to the scientific basis of reactor control and safety under various operating conditions.

5.4. Temperature reactivity coefficient

This chapter evaluates the effect of temperature, ensuring reactor safety under various temperature conditions. The experimental process included 10 data sets, each consisting of five temperature increase and five temperature decrease steps, measured with 14 thermocouples to

obtain the average outlet coolant temperature. The main stages of the experiment involved changing the sodium temperature in the reactor active core to the specified value and maintaining it constant. Control rods were withdrawn to achieve the critical state and then reintroduced until reactor shutdown, this process was repeated for each temperature level. Additional information regarding the temperature levels reached and the exact positions of the control assemblies is provided in Table 5.4 [20].

Table 5.4. Measurements Regarding the Temperature Effect.

Process	Temperature (°C)	Control rod position* [mm]				
		RE1	RE2	SH1	SH2	SH3
increasing	250	207.2	207.7	247.9	247.7	248.0
	275	212.3	212.9	253.6	253.1	253.8
	283	239.7	239.3	253.4	253.1	254.0
	293	282.8	283.4	253.4	253.0	253.7
	302	307.5	307.0	254.7	254.6	255.9
decreasing	300	407.7	408.5	501.5	162.3	162.2
	290	283.4	283.8	254.0	253.7	254.4
	281	285.2	284.6	502.0	162.2	162.2
	270	232.4	232.2	501.9	162.2	162.2
	250	118.5	118.9	501.8	162.2	163.0

**Safety rods are completely withdrawn*

Reactivity measurements were conducted for each temperature level, resulting in eight reactivity values for each temperature interval. The temperature reactivity coefficient was calculated for each temperature increase and decrease process using different evaluation methods [22]:

- *Experimental method* (experiment-dependent): This method involves the exact simulation of the experiment conditions and correcting the reactivity induced by control assemblies using the S-curve.
- *Three-step method:* This method involves summing three reactivities obtained using the following combinations:
  - Temperature and control rod positions of step i,
  - Temperature and control rod positions of step i+1,
  - Temperature of step i+1 and control rod positions of step i.
- *Fixed method*: In this method, all control rods are fully withdrawn, regardless of the reactor's temperature. This represents an assessment of the temperature effect in a scenario where control rods are not used to maintain reactor safety.

The results obtained from simulations using the three-step method and the corresponding experimental data for the temperature increase and decrease processes are presented in Table 5.5.

Table 5.5. Temperature Reactivity Coefficient.

	T	Control rod positions* (mm)					k_{eff}		$\bar{\alpha}$ (Std. dev) [pcm/°C]		Experimental
	(°C)	RE1	RE2	SH1	SH2	SH3	SERPENT 2	MCNP 6.2	SERPENT 2	MCNP 6.2	
Increasing	250	207.2	207.7	247.9	247.7	248.0	1.00410	1.00413			
	275	212.3	212.9	253.6	253.1	253.8	1.00511	1.00502	-3.04 (±0.25)	-3.07 (±0.33)	-3.76
	275	207.2	207.7	247.9	247.7	248.0	1.00434	1.00427			
	283	293.7	293.3	253.4	253.1	254.0	1.00476	1.00463			

	T	Control rod positions* (mm)					k_{eff}		$\bar{\alpha}$ (Std. dev) [pcm/°C]		Experimental
	(°C)	RE1	RE2	SH1	SH2	SH3	SERPENT 2	MCNP 6.2	SERPENT 2	MCNP 6.2	
	283	212.3	212.9	253.6	253.1	253.8	1.00450	1.00435			
	293	282.8	283.4	253.4	253.0	253.7	1.00486	1.00476			
	293	293.7	293.3	253.4	253.1	254.0	1.00456	1.00448			
	302	307.5	307.0	254.7	254.6	255.9	1.00496	1.00503			
	302	282.8	283.4	253.4	253.0	253.7	1.00470	1.00472			
Decreasing process	300	407.7	408.5	501.5	162.3	162.2	1.00397	1.00391			
	290	283.4	283.8	254.0	253.7	254.4	1.00438	1.00433			
	290	407.7	408.5	501.5	162.3	162.2	1.00472	1.00463			
	281	285.2	284.6	502.0	162.2	162.2	1.00350	1.00345			
	281	283.4	283.8	254.0	253.7	254.4	1.00378	1.00373	-3.14 (±0.25)	-3.02 (±0.34)	-4.38
	270	232.0	232.0	501.0	162.0	162.0	1.00327	1.00328			
	270	285.2	284.6	502.0	162.2	162.2	1.00367	1.00360			
	250	118.5	118.9	501.8	162.2	162.0	1.00270	1.00257			
	250	232.0	232.0	501.0	162.0	162.0	1.00325	1.00319			

Discrepancies between simulations with SERPENT 2 and MCNP 6.2 and experimental data were identified, suggesting possible issues related to the "tmp" cards used and the nuclear data available in the ENDF/B.VIII.0 library. Solutions were proposed to correct these discrepancies, including the use of nuclear data libraries at specific temperatures and rechecking input files.

An important step in eliminating the discrepancies was using the auxiliary program MAKXSF [23] to generate nuclear data at the exact temperatures of the experiment. The results obtained with this method are presented in Table 5.6 and indicate a significant improvement in concordance with experimental data, highlighting the importance of using this approach to precisely assess the temperature effect in sodium-cooled reactors.

Table 5.6. Temperature Reactivity Coefficient using MCNP 6.2.

Temperature (°C)	α (Std. dev.) [pcm/°C]			
	Experimental	Method 1	Method 2	Method 3
Increasing process (250°C - 302°C)	-3.76(±0.50)	-3.57 (±0.29)	-3.40 (±0.86)	-3.48 (±0.28)
Decreasing process (300°C - 250°C)	-4.38(±0.57)	-3.55 (±0.29)	-3.46 (±0.84)	-3.51 (±0.28)

5.5. Void reactivity

The chapter analyzes the assessment of the void effect, a crucial aspect of nuclear security. The void effect refers to reactivity changes in the absence or loss of the coolant (sodium). The experiment involves replacing the fuel assembly with a special one to measure void reactivity at five distinct locations in the fuel assemblies. Important parameters, such as sodium temperature and control assembly positions, are recorded in real-time. Details relevant to void reactivity measurement are presented in Table 5 7 [20].

Table 5.7. Parameters of interest for void reactivity measurement.

Position		T (°C)	Control rod position (mm)	
			RE1	RE2
(2-4)	Original	248	277.6	277.3
	Void	247	336.8	336.8
(3-7)	Original	248	278	277.4
	Void	248	337.9	337.9
(4-9)	Original	248	277.7	277.6
	Void	248	338	337.6
(5-11)	Original	248	278.4	276.2
	Void	248	338	337.5
(6-13)	Original	248	302.9	303.3
	Void	248	338.1	337.8

The experiment reveals that, under void conditions, the sodium-cooled fast reactor exhibits negative reactivity, confirmed by withdrawing control rods to achieve criticality.

The assessment of void reactivity can be carried out using multiple computational approaches, such as [22]:

- *Experimental Method:* This method involves considering various configurations of control rods within the experiment, including their positions in the original configuration and in the configuration with the specially designed assembly for the experiment. Void reactivity can be determined through experimental measurements and modifications to these configurations.
- *Fixed Method:* In this approach, control rods are completely extracted, simulating a situation where they are no longer in operation or are removed from the reactor.

The results obtained for void reactivity assessment using the SERPENT 2 and MCNP 6.2 codes and comparison with experimental data are presented in Figure 5.5.

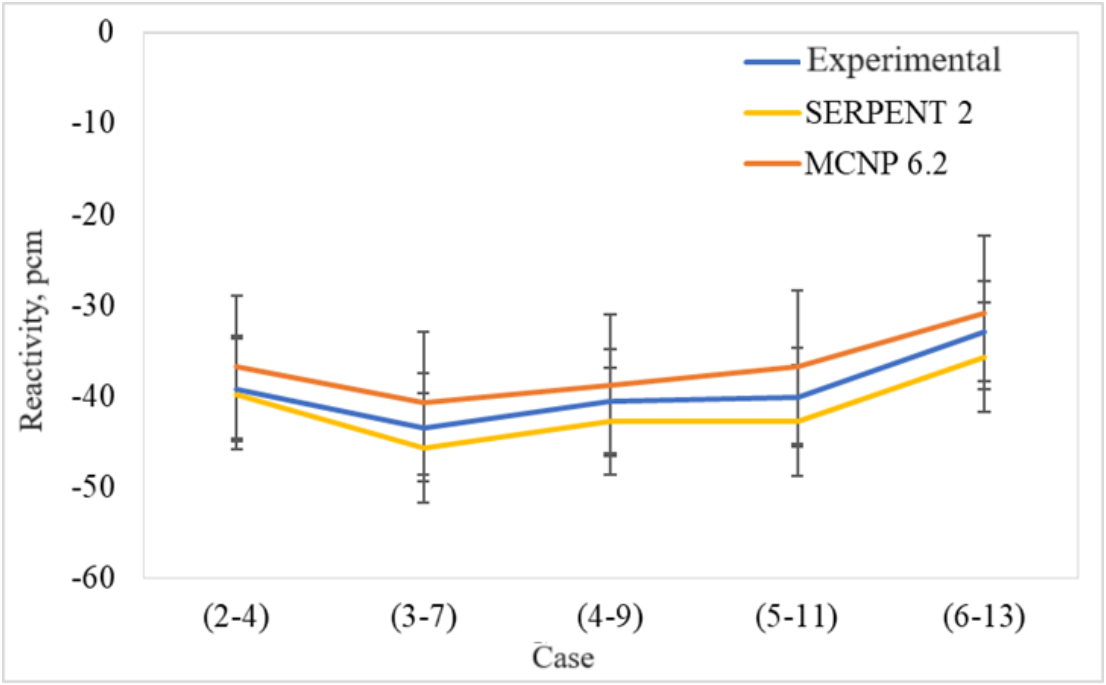

Figure 5.5: Void reactivity assessment using the SERPENT 2 and MCNP 6.2 codes.

The simulations are consistent and close to experimental values, providing essential insight into the reactor's behavior in coolant loss scenarios. However, the analysis reveals significant differences between the results of SERPENT 2 and MCNP 6.2, prompting an additional verification of the MCNP 6.2 input file. Recalibrating the simulations improves their agreement and accuracy, which is crucial for validating computational models.

The results obtained from these additional simulations are presented in Figure 5.6.

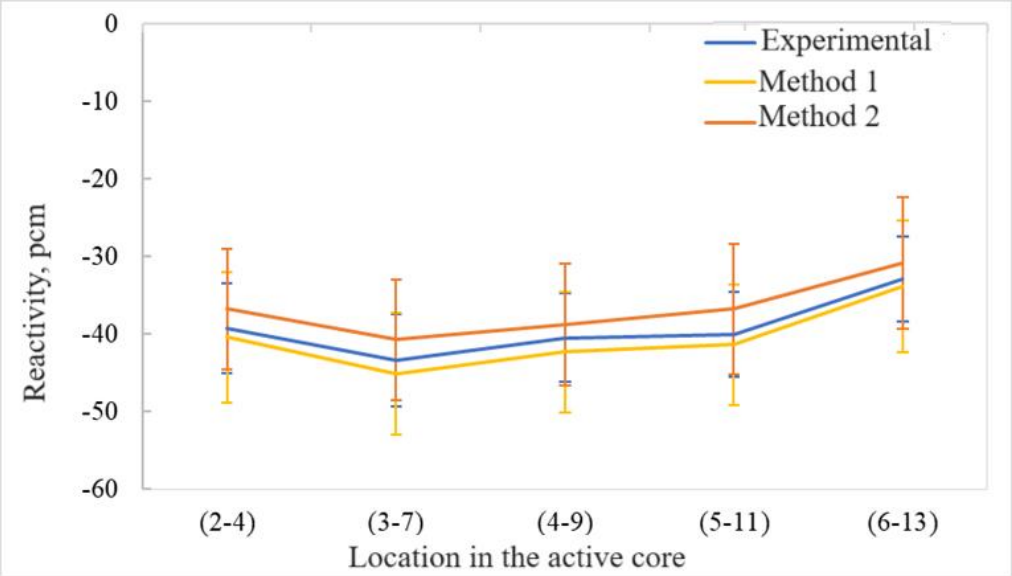

Figure 5.6: Void reactivity assessment using MCNP 6.2.

The conclusions drawn contribute to understanding reactivity effects during coolant loss and developing intervention strategies in emergencies. The validation of these simulations is crucial for ensuring the safety and performance of the sodium-cooled reactor, strengthening confidence in the models used, and supporting nuclear energy as a safe and sustainable source.

5.6. Swap reactivity

This chapter describes an experiment in which measurements were conducted to assess induced reactivity in the case of incorrect fuel loading into a reactor. The experiment involved eight assemblies, six of which were fuel assemblies, and two were steel assemblies. The main objective was to simulate situations where fuel is loaded incorrectly.

The experiment had two distinct phases for fuel and steel assemblies. For fuel assemblies, they were replaced with steel assemblies, and control rods were gradually withdrawn until reaching a controlled critical state. A different logic was used for steel assemblies to keep the reactor safe, avoiding exceeding the critical number of fuel assemblies.

Measurements included assessing reactivity when changing the positions of control rods, both for the movement of a single rod and multiple rods. Experimental results showed that replacing a fuel assembly with a steel one induced negative reactivity while replacing a steel assembly with a fuel one induced positive reactivity.

Simulations using the SERPENT 2 and MCNP 6.2 models exhibited similar behavior to experimental data for single and multiple rod movements but underestimated the measured values. The results obtained are presented in Table 5.8 and Table 5.9, respectively. The

differences can be attributed to incomplete understanding and modeling uncertainties related to the movement and positioning of control rods.

Table 5.8. Swap Reactivity (Single Control Rod).

Position		Control rod position/mm					k_{eff}		$\Delta\rho$ (Std. dev.) [pcm]		Experimental
		RE1	RE2	SH1	SH2	SH3	SERPENT	MCNP	SERPENT	MCNP	
(2-6)	Before	267.7	267.5	287.1	286.4	150.9	1.00358	1.00342	-883 (±7.44)	-871 (±10.39)	-984 (±128)
	After	238.5	237.6	286.6	286.4	341.8	1.00402	1.00401			
	After[*]	267.7	267.5	287.1	286.4	150.9	0.99476	0.99473			
(3-11)	Before	258.2	257.7	267.4	267.4	188.9	1.00348	1.00339	-787 (±7.44)	-791 (±8.65)	-875 (±114)
	After	258.9	258.4	267.2	267.4	353.4	1.00381	1.00369			
	After[*]	258.2	257.7	267.4	267.4	188.9	0.99561	0.99549			
(4-17)	Before	257.8	257.2	267.3	267.4	188.4	1.00348	1.00344	-696 (±7.44)	-697 (±9.84)	-772 (±100)
	After	258.3	257.8	267.5	268.4	333.9	1.00396	1.00378			
	After[*]	257.8	257.2	267.3	267.4	188.4	0.99653	0.99647			
(5-23)	Before	258.2	257.7	265.2	265.6	193.3	1.00336	1.00344	-560 (±7.44)	-573 (±10.38)	-639 (±83)
	After	258.2	257.1	265.1	265.6	303.1	1.00244	1.00218			
	After[*]	258.2	257.7	265.2	265.6	193.3	0.99776	0.99770			
(6-29)	Before	257.1	259.6	266.8	266.2	190.3	1.00348	1.00337	-399 (±7.43)	-396 (±9.82)	-476 (±62)
	After	298.5	297.5	266.8	266.8	299.5	1.00555	1.00550			
	After[*]	257.1	259.6	266.8	266.2	190.3	0.99948	0.99940			
(5-22)	Before	298.4	299.6	266.8	266.8	299.6	1.00361	1.00356	-517 (±7.32)	-529 (±10.37)	-586 (±76)
	After	229.6	230.3	266.5	266.2	207.5	1.00410	1.00408			
	After[*]	298.4	299.6	266.8	266.8	299.6	0.99843	0.99826			
(7-31)	Before	258.2	257.7	262.3	262.6	197.5	1.00552	1.00546	189 (±7.24)	182 (±9.8)	210 (±27)
	After	257.4	257.2	262.1	262.2	285.2	1.00202	1.00200			
	After[*]	258.2	257.7	262.3	262.6	197.5	1.00743	1.00730			
(5-19)	Before	257.4	257.2	262.1	262.2	285.2	1.00244	1.00240	534 (±7.36)	547 (±9.8)	582 (±76)
	After	257.6	257.4	262.2	262.7	247.8	1.00597	1.00599			
	After[*]	257.4	257.2	262.1	262.2	285.2	1.00783	1.00793			

[*]*The configuration of the active core after changing the assembly, but with the positions of the control rods before the change.*

Table 5.9. Swap Reactivity (Multiple Control Rods).

Position		Control rod position/mm					k_{eff}		$\Delta\rho$ (Std. dev.) [pcm]		Experimental
		RE1	RE2	SH1	SH2	SH3	SERPENT	MCNP	SERPENT	MCNP	
(2-6)	Before	267.2	267.3	241.2	242.0	241.4	1.00361	1.00351	-882 (±7.44)	-864 (±9.26)	-986 (±128)
	After	326.7	325.2	297.6	297.2	299.0	1.00385	1.00383			
	After[*]	267.2	267.3	241.2	242.0	241.4	0.99480	0.99488			
(3-11)	Before	257.6	257.1	241.5	241.7	242.0	1.00363	1.00353	-785 (±7.44)	-783 (±10.38)	-880 (±114)
	After	258.2	260.4	293.3	293.4	294.5	1.00378	1.00362			
	After[*]	257.6	257.1	241.5	241.7	242.0	0.99578	0.99571			
(4-17)	Before	258.9	257.2	241.6	241.5	241.3	1.00358	1.0036	-687 (±7.44)	-705 (±10.38)	-777 (±101)
	After	257.1	257.7	288.2	288.9	288.7	1.00391	1.00393			
	After[*]	258.9	257.2	241.6	241.5	241.3	0.99671	0.99655			
(5-23)	Before	257.7	257.1	241.1	241.1	241.3	1.00354	1.00345	-550 (±7.38)	-546 (±10.38)	-634 (±82)
	After	293.4	292.9	275.7	275.0	275.0	1.00240	1.00237			
	After[*]	257.7	257.1	241.1	241.1	241.3	0.99803	0.99798			
(6-29)	Before	258.8	258.9	241.0	242.2	241.8	1.00358	1.00348	-393 (±7.31)	-398 (±9.82)	-474 (±62)
	After	317.9	317.0	277.7	277.2	278.5	1.00571	1.00576			
	After[*]	258.8	258.9	241.0	242.2	241.8	0.99964	0.99949			
(5-22)	Before	319.1	317.2	277.7	277.2	278.6	1.00348	1.00345	-499	-502	-590

Position		Control rod position/mm					k_{eff}		$\Delta\rho$ (Std. dev.) [pcm]		Experimental
		RE1	RE2	SH1	SH2	SH3	SERPENT	MCNP	SERPENT	MCNP	
(7-31)	After	230.0	229.4	247.1	246.6	247.0	1.00399	1.00345	(±7.37)	(±9.26)	(±77)
	After[*]	319.1	317.2	277.7	277.2	278.6	0.99848	0.99842			
	Before	258.1	259.7	241.4	241.2	242.0	1.00583	1.00554	175 (±7.35)	188 (±10.34)	210 (±27)
	After	295.2	294.5	267.6	267.4	268.7	1.00212	1.00196			
	After[*]	258.1	259.7	241.4	241.2	242.0	1.00760	1.00744			
(5-19)	Before	295.2	294.5	267.6	267.4	268.7	1.00240	1.00231	540 (±7.29)	570 (±9.8)	582 (±76)
	After	295.2	294.6	255.3	255.2	255.8	1.00597	1.00598			
	After[*]	295.2	294.5	267.6	267.4	268.7	1.00786	1.00807			

[*] *The configuration of the active core after changing the assembly, but with the positions of the control rods before the change.*

The experiment's conclusions have highlighted the importance of the positions of the control rods and the uncertainties associated with their movement in assessing reactivity during incorrect fuel loading.

5.7. Radial and axial distribution of reaction rate

This chapter focuses on the relative distribution of reaction rates and the experimental measurements conducted to validate computational models and nuclear data used in fast reactor assessments. The measurements involved the use of 202 activation foils, and high-quality results included measurements for various processes such as ^{235}U(n,f), ^{238}U(n,f), ^{237}Np(n,f), ^{197}Au(n,γ), ^{58}Ni(n,p), ^{27}Al(n,α).

These activation foils were placed in test assemblies loaded in 8 positions (5 for fuel and 3 for steel assemblies). The reaction rate measurement procedure involved a temporary increase in reactor power to achieve the required irradiation power quickly. Measurements were conducted with a high-purity germanium spectrometer, and the results were normalized.

For evaluating reaction rates, "F4" and "FM" cards within the MCNP 6.2 code were utilized. These provided axial and radial distributions of normalized reaction rates. Figure 5.7 presents the axial distribution of reaction rates, illustrating how reaction rates vary with axial position in the reactor. Additionally, Figure 5.8 depicts the radial distribution of reaction rates, indicating how reaction rates vary with radial distance from the reactor axis.

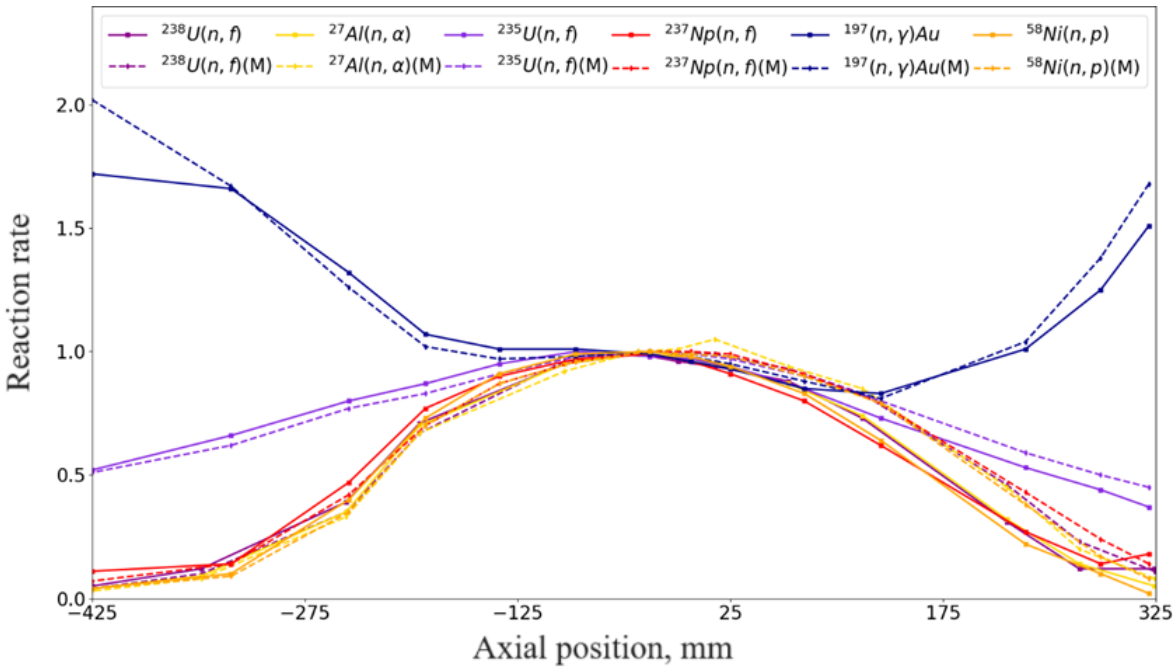

Figure 5.7: Axial Distributions of Reaction Rates.

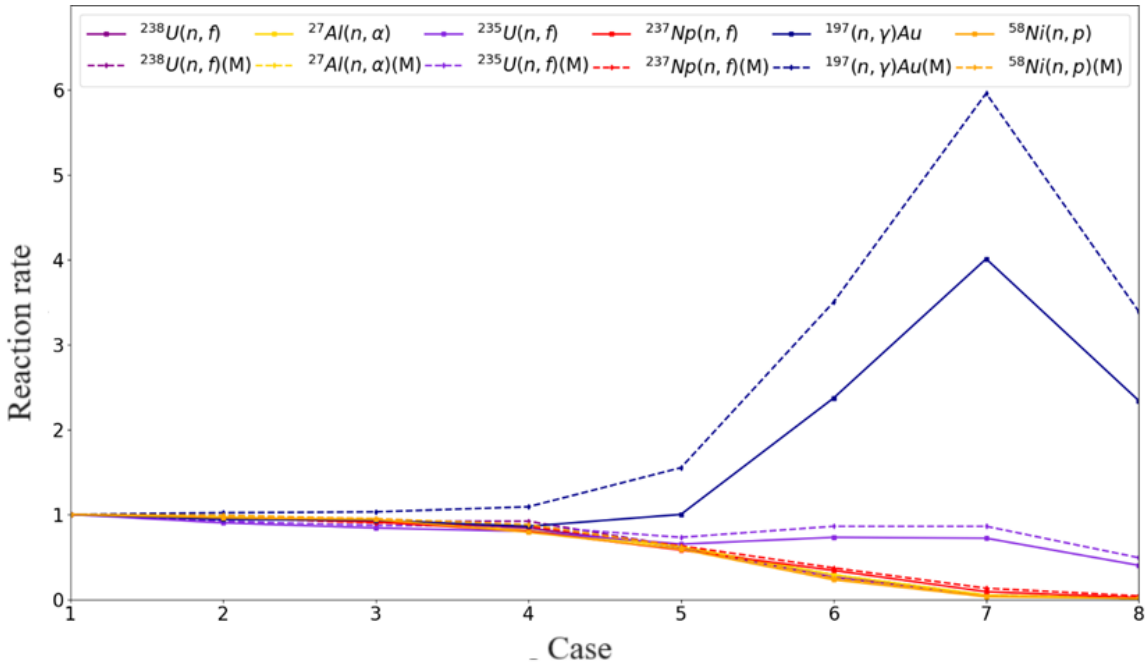

Figure 5.8: Radial Distributions of Reaction Rates.

The simulation results were compared with experimental data, revealing good agreement in most cases, except for the ^{197}Au(n,γ). The differences observed in this case were attributed to resonance energy capture cross-sections and the use of virtual materials in the simulations.

5.8. Nuclear data libraries

This chapter addresses the importance of nuclear data in nuclear physics research, emphasizing them as essential parameters for neutron codes and the primary source of uncertainty [8]. Neutronic simulations rely on nuclear data to provide a precise numerical

representation of physical phenomena, and these data cover an extensive range of neutron energies and approximately 400 atomic nuclei [24].

There are three main categories of nuclear data libraries, classified based on their sources and applications: experimental, evaluated, and applied. Experimental libraries are based on direct measurements, such as those from EXFOR [25], but may not always meet the requirements for advanced systems. Evaluated libraries complement experimental data with theoretical models, while applied libraries are tailored for direct use in neutronic calculation codes.

Over the decades, several nuclear data libraries have been developed, and standardization efforts have been ongoing, albeit with significant differences between evaluations. The main nuclear data libraries today include ENDF/B [26], JEFF [27], JENDL 0 [28], CENDL [29], and BROND [30],, each having its coverage domain and making a significant contribution to nuclear research.

It is important to note that nuclear data are not devoid of uncertainties, which can arise from experiment imperfections or statistical fluctuations. Uncertainties are evaluated and provided as covariance matrices, although uncertainty information is not always available. The ultimate goal is to achieve a common and universally accepted nuclear data library, but this goal has not been fully realized, and significant differences persist between various existing nuclear data libraries.

The work compares five nuclear data libraries (ENDF/B-VIII.0, JEFF3.3, JENDL4.0, CENDL3.1, and BROND3.1) in the context of small sodium-cooled reactors. The main objective is to identify and quantify sources of inconsistencies between these libraries, with a focus on the fast spectrum. The analysis results are presented in Table 5.10, showing the multiplication factors (k_{eff}) obtained for each library compared to experimental results.

Table 5.10. Multiplication Factor Obtained for Different Nuclear Data Libraries.

Nuclear data library	k_{eff}	Std. dev. [pcm]	Δρ [pcm]
ENDF/B-VIII.0	1.00078	6	78
JEFF-3.3	1.00221	5	221
JENDL-4.0	1.00583	5	583
BROND-3.1	1.00433	5	433
CENDL-3.1	1.01291	6	1291
Experimental	1.00000	-	-

All analyzed libraries overestimate the experimental results, with ENDF/B-VIII.0 providing the closest results. Notable differences include the significant overestimation of the multiplication factor for ^{235}U in JEFF3.3 and JENDL4.0 and for ^{23}Na in JENDL4.0 and CENDL3.1.

According to previous analyses, the ENDF/B-VIII.0 library performs well regarding the fast spectrum. However, due to the impact of new evaluations included in ENDF/B-VIII.0, further investigations are necessary to assess the library's performance in the context of multiple isotopes and diverse nuclear systems. In this regard, ENDF/B-VIII.0 is chosen as the reference

library for the analysis of the main isotopes involved in the simulations conducted in the study [31].

Each simulation replaces the data for a specified isotope in ENDF/B-VIII.0 with those from a specified nuclear data library. The differences in reactivity compared to the reference case are presented in Table 5.11, and the provided data include a statistical uncertainty of 5-6pcm each. This approach aims to evaluate the performance of nuclear data libraries for relevant isotopes and quantify the discrepancies between these libraries and the ENDF/B-VIII.0 library.

Table 5.11. Reactivity Induced by Isotope Substitution in ENDF/B-VIII.0.

Isotope	**JEFF3.3**	**JENDL4.0**	**BROND3.1**	**CENDL3.1**
^{10}B	-7.99	10.98	-3.00	4.99
^{11}B	6.99	2.00	6.99	0.00
^{12}C	-2.00	6.99	-5.99	10.98
^{16}O	153.52	192.33	130.62	169.45
^{23}Na	174.42	380.95	80.81	374.01
^{29}Si	0.00	-2.00	0.00	6.99
^{54}Fe	3.99	-3.99	3.99	-3.99
^{56}Fe	-125.96	10.98	11.98	-287.38
^{57}Fe	115.69	88.78	-73.94	103.73
^{58}Fe	9.98	-6.99	3.00	-3.99
^{58}Ni	267.86	62.86	178.40	-8.99
^{60}Ni	232.10	76.82	40.92	15.97
^{61}Ni	-9.99	-2.00	-6.99	-1.00
^{62}Ni	-6.99	-10.98	5.99	-27.96
^{64}Ni	184.37	-3.99	-6.99	10.98
^{235}U	-529.97	-385.88	42.91	178.40
^{238}U	177.41	-63.94	28.95	-36.96
U	-377.84	-440.25	61.87	130.62

The conclusion is that selecting an appropriate nuclear data library is crucial for obtaining accurate simulations, and uncertainty analyses are essential for quantifying the uncertainties associated with nuclear data and simulation models. This contributes to achieving robust results and the precise evaluation of the behavior of the reactor or other systems involving nuclear reactions.

6. CONCLUSION

6.1. General conclusion

The work is organized into six chapters, each addressing specific aspects of research on the sodium-cooled fast reactor, focusing on the CEFR reactor. These sections include:

- An overview of the role of nuclear energy in the global energy mix and the presentation of fast reactors, with an emphasis on sodium-cooled reactors, such as the CEFR reactor.
- Coverage of neutron transport theory and detailed explanations of the calculation codes used in simulations, particularly SERPENT 2 and MCNP 6.2.
- Explanations about reactivity effects in fast reactors.
- A detailed description of the CEFR reactor model used.
- Presentation of the developed models and the results obtained from simulations.

The thesis focuses on neutron simulations in the context of the CEFR reactor (China Experimental Fast Reactor). The primary goal of this research was to predict neutron behavior in the reactor under static conditions, addressing various critical parameters. Simulations included aspects such as effective multiplication factor, radial power distribution, reactivity induced by control systems, reactivity effects (including void reactivity and temperature reactivity), reaction rates, and evaluating nuclear data libraries.

Two Monte Carlo codes, SERPENT 2 and MCNP 6.2, were successfully used for essential neutron analyses. Simulations involved the complex modeling of reactor geometry and assemblies, and the results were validated compared to experimental data. This highlighted the importance of international collaboration in energy and nuclear research.

The research included simulating the transition process from subcritical to critical state in the sodium-cooled reactor, with results showing consistency between simulations and experimental data. Additionally, the effectiveness of control systems was evaluated, emphasizing their importance for the safe operation of the reactor.

Simulations for temperature effects initially revealed significant underestimations, which were later corrected with the help of the auxiliary program MAKXSF. The evaluation of void reactivity and the swap reactivity provided consistent results.

The study also assessed nuclear data libraries, highlighting discrepancies between their estimates and experimental results. The good performance of the ENDF/B-VIII.0 library for fast spectrum reactors is emphasized, but the need for further investigations is noted.

In conclusion, this work contributes significantly to nuclear reactor research, highlighting the importance of precise numerical simulations, code validation, and the appropriate selection of nuclear data libraries. The research opens new directions for the future and underscores the complexity and importance of this vital field.

6.2. Personal contribution

In this work, I have made significant contributions and undertaken several essential activities:

Choice of Calculation Codes: I selected the calculation codes used in neutron simulations. After careful evaluation, I chose the SERPENT 2 and MCNP 6.2 codes. The study utilized these to model the CEFR reactor and simulate reactor start-up tests.

Modeling of the CEFR Reactor: I developed complex 3D models of the CEFR reactor, considering its detailed geometry, materials used, and the distribution of components. This effort included a detailed representation of fuel assemblies, control assemblies, and other critical reactor elements.

Neutronic Simulations for Criticality Analyses: I conducted neutron simulations using the SERPENT 2 and MCNP 6.2 codes to assess the effective multiplication factor of the CEFR reactor. Significant efforts were made to ensure the validity and accuracy of the simulations, contributing to a detailed understanding of neutron behavior in the reactor.

Analysis of Reactivity Effects: I investigated and analyzed reactivity effects associated with temperature changes, such as the Doppler effect, thermal expansion, and changes in material density within the reactor. These analyses provided essential information for evaluating these effects' impact on the reactor's safety and stability.

Evaluation of Nuclear Data: I thoroughly evaluated various nuclear data libraries to determine their impact on neutron simulations. Analyzing and comparing reactivity using different libraries contributed to identifying discrepancies and highlighting the importance of validating this data in CEFR reactor simulations.

Comparison of Results with Experimental Data: I rigorously compared simulation results with available experimental data. This step contributed to the validation and verification of neutron simulations, ensuring the precision and accuracy of the obtained results.

Contributions to Nuclear Safety Analyses: My research significantly impacted nuclear safety by developing and validating neutronic simulation models for the CEFR reactor. This contributed to a deeper understanding of neutron behavior in reactors and identifying solutions to enhance the safety and efficiency of these systems.

Through these contributions, I have added significant value to developing knowledge and research in nuclear reactors and neutron analyses. My work has substantially improved the understanding of nuclear phenomena, safety, and efficiency of the CEFR reactor, as well as the validation of nuclear data used in reactor simulations. These contributions have significantly impacted the field of nuclear reactor research and safety in general.

6.3. Future perspective

The prospects for this work are promising and encompass several relevant directions:

Continuation of CEFR Reactor Research: The work provides a solid foundation for further investigations into the behavior of the CEFR reactor under various operating conditions. It can serve as a starting point for enhancements in this reactor's performance, safety, and

efficiency or other similar fast reactors. Additionally, the continuation of studies on other tests conducted within the CEFR reactor has been established, expanding the scope of research.

Development of Advanced Models: The work can continue to contribute to developing and refining models used for CEFR reactor simulations. This may involve improving existing models and extending them to include thermal-hydraulic models or any other aspect relevant to reactor operation.

Safety and Security Analyses: An important future direction could involve expanding the work to include detailed safety analyses. This might entail identifying and evaluating potential risks associated with reactor operation and developing solutions to manage them, with a particular focus on reactor safety.

Extended Validation and Verification: Continuing efforts in validating and verifying calculation codes and simulations are essential to ensure the accuracy and relevance of results under real reactor operating conditions.

Application to Similar Projects: The expertise gained and the results of this work can be successfully applied to similar fast reactor projects in other countries or organizations. Knowledge transfer can contribute to advancing research in nuclear reactors on a global scale.

International Collaboration: Ongoing collaboration with international experts and research organizations in the field of nuclear reactors can bring significant benefits. The exchange of ideas and experiences can stimulate innovation and contribute to the overall research progress in this complex and vital domain.

By addressing these directions, this work can continue to make significant contributions to the field of nuclear reactors and neutron simulations, advancing knowledge and improving existing technologies.

BIBLIOGRAFY

[1] V. Masson-Delmotte, et. al., „Climate Change 2021 The Physical Science Basis," IPCC - Intergovernmental Panel on Climate Change.

[2] M. Alwaeli și V. Mannheim, „Investigation into the Current State of Nuclear Energy and Nuclear Waste Management—A State-of-the-Art Review," *Energies,* vol. 15, 2022.

[3] „Nuclear Power Reactors in the World," IAEA - International Atomic Energy Agency, 2022.

[4] „GIF 2021 Annual Report," 2021.

[5] I. l. Pioro, Handbook of Generation IV Nuclear Reactors, Woodhead Publishing Series in Energy, 2016.

[6] Overview of Generation IV (Gen IV) Reactor Designs. Safety and Radiological Protection Consideration, IRSN, 2012.

[7] T. Takeda, „Minor actinides transmutation performance in a fast reactor," *Annals of Nuclear Energy,* 2016.

[8] D. G. Cacuci, Handbook of Nuclear Engineering: Nuclear Engineering Fundamentals, Springer, 2010.

[9] J. R. Lamarsh, Introduction to Nuclear Reactor Theory, New York: Addison-wesley Publishing Company, 2002.

[10] B. Zohuri, Neutronic Analysis For Nuclear Reactor Systems, Switzerland: Springer Nature, 2016.

[11] L. Cao și H. Wu, Deterministic Numerical Methods for Unstructured-Mesh Neutron Transport Calculation, Woodhead Publishing, 2020.

[12] F. Brown, *Monte Carlo Techniques for Nuclear Systems – Theory Lectures,* LA-UR-16-29043.

[13] A. Moise, I. Vișan și A. Rizoiu, „Evaluation of TH-based CANDU 6 Fuel Bundle Performance using MONTE CARLO and Collision Probability Methods," *Journal of Nuclear Research and Development,* nr. 18, pp. 39-42, 2019.

[14] T. K. Kim, et. al., „Benchmark Comparisons of Deterministic and Monte Carlo Codes for a PWR Heterogeneous Assembly Design," în *The Physics of Fuel Cycles and Advanced Nuclear Systems: Global Developments - PHYSOR2004,* 2004.

[15] M. V. Shchurovskaya, et. al., „Validation of deterministic and Monte Carlo codes for neutronics calculation of the IRT-type research reactor," în *IOP Conference Series: Journal of Physics,* 2017.

[16] J. Leppänen, „Serpent – a Continuous-energy Monte Carlo Reactor Physics Burnup Calculation Code. User's Manual," 2013.

[17] „Monte Carlo N-Particle Transport Code System Version 6.2," Los Alamos National Laboratory, 2017.

[18] M. Weston, Nuclear Reactor physics, Wiley-VCH, 2007.

[19] X. Yang et al., „The first criticality test of CEFR," în *Proceedings of the 2013 21st International Conference on Nuclear Engineering,* Chengdu, 2013.

[20] CIAE, „Neutronics Benchmark of CEFR Start-Up Tests. Draft V7.0," 2020.

[21] Gomez Torres A. M., et al., „Verification and validation of neutronic codes using the start-up fuel load and criticality tests performed in the China Experimental Fast Reactor," în *The 22th International Conference on Fast Reactors and Related Fuel Cycles: Sustainable Clean Energy for the Future*, 2022.

[22] A. Moise, D. Dupleac și I. Visan, „Evaluation of the Reactivity Feefback in a Liquid Metal-Cooled Fast Reactor," *UBP Scientific Bulletin,* 2022.

[23] F. B. Brown, „The makxsf Code with Doppler Broadening," Los Alamos National Laboratory, LA-UR-06-7002, 2006.

[24] A. Foderaro, The Elements of Neutron Interaction Theory, MIT Press, 1971.

[25] Otuka N et. al., „Towards a more complete and accurate experimental nuclear reaction data library (EXFOR): international collaboration between nuclear reaction data centers (NRDC)," *Nuclear Data Sheets,* nr. 120, 2014.

[26] BROWN, D. A. ET AL., „ENDF/B-VIII.0: The 8th major release of the nuclear reaction data library with CIELO-project cross sections, new standards and thermal scattering data," *Nuclear Data Sheets,* vol. 148, pp. 1-142, 2018.

[27] PLOMPEN, A. J. M. ET AL., „The joint evaluated fission and fusion nuclear data library, JEFF-3.3," *The European Physical Journal A,* vol. 56, nr. 181, 2020.

[28] SHIBATA, K. ET AL., „JENDL-4.0: A new library for nuclear science and engineering," *Journal of Nuclear Science and Technology,* vol. 48, nr. 1, pp. 1-30, 2011.

[29] Z. G. Ge et al., „The Updated Version of Chinese Evaluated Nuclear Data Library (CENDL-3.1)," *Journal of the Korean Physical Society,* vol. 56, nr. 2, pp. 1052-1056, 2011.

[30] A.I. Blokhin et, al, „New version of neutron evaluated data library BROND-3.1," *Yad.Reak.Konst,* nr. 2, p. 62, 2016.

[31] A. Moise și I. Visan, „Neutronic Calculation of CEFR core using different nuclear data libraries," în *The 22th International Conference on Fast Reactors and Related Fuel Cycles: Sustainable Clean Energy for the Future*, Viena, 2022.